REPORT DOCUMENTATION PAGE			Form Approved OMB No. 0704-0188

1. AGENCY USE ONLY *(Leave blank)*	2. REPORT DATE	3. REPORT TYPE AND DATES COVERED
	14 November 1996	Scientific No. 3

4. TITLE AND SUBTITLE	5. FUNDING NUMBERS
Survey of Experimental Results From One Year of PASP PLUS Orbital Operation	PE 63410F PR S321 TA GY WU AC
6. AUTHOR(S) D. A. Guidice* J. R. Palys H.B. Curtis** M. F. Piszczor**	Contract F19628-93-K-0019
7. PERFORMING ORGANIZATION NAME(S) AND ADDRESS(ES) Boston College Institute for Scientific Research Newton, MA 02159-1164	**8. PERFORMING ORGANIZATION REPORT NUMBER**
9. SPONSORING/MONITORING AGENCY NAME(S) AND ADDRESS(ES) Phillips Laboratory 29 Randolph Road Hanscom AFB, MA 01731-3010 Contract Manager: Alan Griffin/GPD	**10. SPONSORING/MONITORING AGENCY REPORT NUMBER** PL-TR-96-2286

11. SUPPLEMENTARY NOTES

* Phillips Laboratory/GPSG, 29 Randolph Road, Hanscom AFB, MA 01731-3010; ** NASA Lewis Research Center, Cleveland, OH

Reprinted from 27th AIAA Plasmadynamics & Lasers Conference, 17-20 Jun 1996, New Orleans, LA

12a. DISTRIBUTION AVAILABILITY STATEMENT	12b. DISTRIBUTION CODE
Approved for public release; distribution unlimited	

13. ABSTRACT *(Maximum 200 words)*

With PASP Plus as its primary payload, the APEX satellite was launched by a standard Pegasus rocket released from a NASA B-52 aircraft on 3 August 1994. A 70° inclination, 363 km × 2550 km orbit was achieved, allowing both investigation of space plasma effects on high-voltage operation in the perigee region and investigation of space radiation effects on array power output from passage through the inner radiation belt in the apogee region. Data gathering by PASP Plus was begun on 7 Aug 94 and ended on 11 Aug 95. In one year, PASP Plus collected an order of magnitude more data on environmental interactions on solar arrays than all previous space-borne photovoltaic experiments combined. The test arrays flown and the interactions-measuring and space-environment sensors of PASP Plus are described. The results of measurements of leakage current under test-array positive biasing and arc rates under negative biasing as a function of bias voltage, plasma density, array orientation, and other conditions are presented. The results of measurements of test-array power-output degradation caused by space radiation are also examined.

14. SUBJECT TERMS		15. NUMBER OF PAGES
PASP PLUS	Space radiation effects	
APEX satellite	Bias voltage	**16. PRICE CODE**
Space plasma effects	Plasma density	

17. SECURITY CLASSIFICATION OF REPORT	18. SECURITY CLASSIFICATION OF THIS PAGE	19. SECURITY CLASSIFICATION OF ABSTRACT	20. LIMITATION OF ABSTRACT
Unclassified	Unclassified	Unclassified	SAR

PL-TR-96-2286

AIAA 96-2331
Survey of Experimental Results from One Year of PASP Plus Orbital Operation

D.A. Guidice
Phillips Laboratory
Hanscom AFB, MA

H.B. Curtis and M.F. Piszczor
NASA Lewis Research Center
Cleveland, OH

J.R. Palys
Boston College
Chestnut Hill, MA

19961118 038

27th AIAA Plasmadynamics and Lasers Conference
June 17-20, 1996 / New Orleans, LA

SURVEY OF EXPERIMENTAL RESULTS FROM ONE YEAR OF PASP PLUS ORBITAL OPERATION

D.A. Guidice
Phillips Laboratory, Geophysics Directorate
Hanscom AFB, Massachusetts

H.B. Curtis, M.F. Piszczor
NASA Lewis Research Center
Cleveland, Ohio

J.R. Palys
Boston College
Chestnut Hill, Massachusetts

Abstract

With PASP Plus as its primary payload, the APEX satellite was launched by a standard Pegasus rocket released from a NASA B-52 aircraft on 3 August 1994. A 70° inclination, 363 km × 2550 km orbit was achieved, allowing both investigation of space plasma effects on high-voltage operation in the perigee region and investigation of space radiation effects on array power output from passage through the inner radiation belt in the apogee region. Data gathering by PASP Plus was begun on 7 Aug 94 and ended on 11 Aug 95. In one year, PASP Plus collected an order of magnitude more data on environmental interactions on solar arrays than all previous space-borne photovoltaic experiments combined. The test arrays flown and the interactions-measuring and space-environment sensors of PASP Plus are described. The results of measurements of leakage current under test-array positive biasing and arc rates under negative biasing as a function of bias voltage, plasma density, array orientation, and other conditions are presented. The results of measurements of test-array power-output degradation caused by space radiation are also examined.

Background

Photovoltaic systems are the preferred method of satisfying the electric power requirements for DoD and commercial space missions. Reasons for this choice include the inexhaustible supply of energy coming from the sun, the relatively light weight and the reliability of solar array subsystems, and the environmentally "clean" form of space power they supply.

Access to space is becoming broader with the advent of greater commercialization, increased communication requirements, and the introduction of a variety of new "small-sat" launch vehicles. While access to space is a privilege exploited by a greater number of users, the cost of acquiring this access is still high and greatly depends on overall mission complexity and spacecraft size. As a means of lowering spacecraft weight, users are considering operating their photovoltaic networks at higher voltages, so that more efficient power distribution subsystems can be used to minimize overall cable losses and/or reduce cable weight. In addition, a variety of new, advanced-technology solar cell materials and manufacturing techniques are being developed, stressing lighter weight and lessened susceptibility to space radiation.

Photovoltaic power systems will continue to prevail as the preferred choice for space power for the foreseeable future. They are not, however, without limitations that must be considered for any space application. Foremost among these limitations is the unavoidable interactions with the hazardous space environment in which they will operate. To understand these limitations, more information must be gathered before new photovoltaic technologies are put into use on operational spacecraft.

Laboratory simulations of space-environment interaction effects on solar arrays have been accomplished on a limited basis.[1,2] However, because of the complex and changing nature of the space environment, these ground tests are inadequate to quantify these effects. The

Photovoltaic Array Space Power Plus Diagnostics (PASP Plus) spaceflight experiment was developed to acquire the needed flight test data. When originally conceived in 1985, the experiment consisted of four solar arrays and limited diagnostic instrumentation for short-term investigation of high voltage/space plasma interactions at Shuttle altitudes. In early 1990, the Air Force's Space Test Program (STP) offered the PASP Plus experiment a flight on the Advanced Photovoltaic and Electronics Experiments (APEX) satellite. Because of the expanded opportunity provided by APEX's elliptical orbit and 1-3 year lifetime, it was decided to broaden the scope of PASP Plus to include the investigation of the effects of space radiation dose on long-term solar array power output. We also added diagnostic instruments appropriate to PASP Plus's new mission profile.[3]

PASP Plus Objectives

The objectives of the PASP Plus experiment were:

(1) Measure the plasma "leakage" current for different kinds of arrays subjected to positive biasing levels up to +500 V.

(2) Measure the arcing parameters for the different kinds of arrays subjected to negative biasing levels up to −500 V.

(3) Measure the long-term degradation in the power output of arrays using different solar-cell materials when exposed to space radiation.

(4) Establish cause-and-effect relationships between array interactions and environmental conditions.

Experiment Instrumentation

The experiment consists of:

(1) A set of test arrays, some of which are divided into biased and unbiased segments.

(2) Experiment-control and interactions-measuring instruments that *create* array (or spacecraft) conditions leading to interactions and *measure* parameters of the interactions that occur.

(3) Diagnostic sensors to measure the ambient environmental conditions causing the interactions or affecting their severity.

Solar Arrays

The 12 PASP Plustest arrays were subdivided into 16 electrically separate modules, 10 of which were subjected to positive and negative biasing. Two of the planar arrays had wrap-through connectors. Three arrays (two planar and one concentrator) featured dual-junction solar cells. See Table I below.

Table I. PASP Plus Solar Arrays

Mod. No.	Cell / Array Type	Number of cells	Cell Size (cm × cm)
0,1,2	Si (Std), 8 mil	20,20,60	2 x 4
3	Si, 8 mil wtc [Space Sta]	4	8 x 8
5	Si, 2 mil [APSA]	14	2.6 x 5.1
9	Amorphous Si	2	4 x 4
4,6	GaAs on Ge, 3½ mil	20,12	4 x 4
8	GaAs on Ge, 7 mil, wtc	4	4 x 4
11	GaAs on Ge, 7 mil	8	4 x 4
7	AlGaAs//GaAs	20	2 x 2
10	InP, 12 mil	10	2 x 2
12,13	GaAs//Cu$InSe_2$	12, 3	2 x 2, 2 x 4
14	GaAs Mini-Cass	8	Concentrator
15	GaAs//GaSb Mini-Dome	12	Concentrator

wtc = wrap-through connectors
// = dual-junction solar cells
underlined module = biased

A brief description of the PASP Plus test arrays was given by Guidice et al.[4] A detailed description, which included cell and array configuration drawings and color photographs of the arrays, was presented in a report by Adams.[5]

Interactions Control/Measurement Instruments

Array Biasing Network: The PASP Plus controller generated and applied to any of the ten arrays (as commanded) a set of four all-positive or all-negative bias steps ranging from 50 to 500 Volts, with a resolution of roughly 4 Volts in that range. The biasing sequence took two minutes; each of the four 30-sec steps consists of 7 seconds of no bias (used for Langmuir Probe and I-V curve measurements) and 23 seconds of biasing. For both positive and negative biasing, there were seven pre-programmed sequences (including one all-zero) and one fully programmable (by ground command) sequence, which was used most of the time. Biases were applied to a module so as to add to its generated voltage; however, in almost all cases, the generated voltage was short circuited.

Electrometer: The electrometer located within the controller is used to measure the leakage current from the space plasma. It covers the range from 0.2 μA to 20 mA with a resolution of 0.2 μA.

Electron Emitter: It produces a stream of *outgoing* electrons to help balance the *incoming* flow of electrons to the biased module during positive biasing, thereby averting the negative charging of the satellite and the negative potential contours around it. However, it was found that when the emitter was on (only during positive biasing), it interfered with the Langmuir Probe measurements of plasma density, which are essential to our leakage current investigation. No extensive analysis of *emitter-on* positive biasing data has been made.

Transient Pulse Monitor (TPM): The TPM consists of a central processing unit, four electromagnetic transient sensors (E-field sensors for detection of radiated pulses) and one current-loop sensor around the high-voltage line inside the controller (for detection of power-line pulses). The TPM measured the properties (amplitude, derivative, integral) of the largest pulse in each one-second interval and the number of pulses (up to 15) in that interval. The TPM was used to obtain the arc rate and characteristics of arc-discharge pulses that occur during negative biasing of the test arrays.

Diagnostic Sensors

Langmuir Probe (LP): The Langmuir Probe measures the parameters (density and temperature) of the space plasma environment in front of the test arrays. To sweep the appropriate voltage range with respect to the space plasma, the LP was equipped with a so-called "senpot", capable of sensing how far negative the satellite frame-ground is below space-plasma reference and compensating for this deviation up to about −30 Volts. When biasing is taking place, the LP makes its measurements during the 7 seconds of the 30-sec biasing interval when the bias voltage is not applied.

Electrostatic Analyzer (ESA): The ESA measures the energetic-particle density of electrons and positive ions (separately) in 20 logarithmically spaced bins over the energy range of 30 eV to 30 keV. The ESA can be used to detect the passage of APEX satellite through an enhanced auroral region. In addition, the lower-energy portion (<300 eV) of the ion spectrum can be used to determine the negative potential of the satellite during high-voltage positive biasing.

Sun Sensor: The sun incidence-angle sensor measures the angles (on two orthogonal axes) between the normal to the array surfaces and the direction to the sun. While in sunlight, the satellite pointed the test arrays to within $\pm 0.5°$ of the center of the sun.

Dosimeter: The dosimeter is used to measure the high-energy particle flux and dose from protons and electrons that lead to degradation in solar-array power output. Its interface (power, command, telemetry) is separate from the PASP Plus controller. Table II gives some of its detection characteristics.

Table II. Electron and Proton Energy Ranges for the PASP Plus Dosimeter

Dome	Aluminum Shield g/cm^2	Aluminum Shield Shape	Electron Threshold (MeV)	Proton Energy (MeV)
D1	0.0294	flat	0.15	5 − 80
D2	0.55	hemisphere	1.0	20 − 115
D3	1.55	hemisphere	2.5	32 − 120
D4	3.05	hemisphere	5.0	52 − 125

Contamination Monitors: Sensors included both quartz crystal microbalances and calorimeters. No significant effects on array performance have been attributed to contamination.

Data Collection

Data collection involving I-V curves and positive and negative biasing of the PASP Plus arrays took place over most of the period from 7 Aug 94 to 11 Aug 95, with several long gaps (e.g., 4 Nov 94 to 15 Jan 95 and 17 May to 1 Jul 95) due to APEX subsystem problems. On 12 Aug 95, a PASP Plus controller hardware malfunction resulted in the end of all biasing operations and taking of I−V curves. The dosimeter was separately interfaced to the satellite and therefore unaffected by this problem. An interrogator problem on APEX curtailed dosimeter data gathering in the fall of 1995. This was corrected, and telemetering of dosimeter data resumed about mid-Dec 1995 and continued into 1996. Summaries of the PASP Plus data collecting for positive and negative biasing operations are given in Tables III and IV.[6]

Table III. Summary of PASP Plus Positive Biasing Operations

Biasing Period	Voltage Range	Plasma Density (cm^{-3})	Environment and Operations Comments
7 Aug - 18 Aug 94	+75 V to +500 V	$6\times10^3 \rightarrow 1\times10^5$ (2×10^5 rare)	Bias $\pm$20 min around perigee. Ram angle at perigee $\leq$90° until 15 Aug. No eclipses over 7-17 Aug. All biasing in sunlight. Emitter on 1/3 of orbits after 11 Aug.
10 Oct - 16 Oct 94	+100 V to +300 V	$6\times10^2 \rightarrow 2\times10^5$	Biasing around perigee. Ram angle at perigee $\geq$90° and no eclipses for whole period. Emitter on about 1/3 of orbits.
24 Oct - 30 Oct 94	+100 V to +320 V	$4\times10^2 \rightarrow 2\times10^5$	Biasing around the orbit. Ram angle at perigee 71°→59° for 24-30 Oct. No eclipse until >28 Oct. Emitter not on.
15 Jan - 17 Jan 95	+75 V to +220 V	$2\times10^3 \rightarrow 6\times10^5$	Biasing only in sunlight. Controller off for altitudes > 1200 km. Ram angle at perigee 106°→97°. Emitter not on.
12 Feb - 2 Mar 95	+50 V to +220 V	$4\times10^2 \rightarrow 3\times10^5$	Biasing 40 min before to 30 min after perigee, but off for alt > 1200 km when near SAA. No eclipse throughout period. Ram angle at perigee 64°→96°. Emitter not on.
27 Apr - 16 May 95	+50 V to +430 V	$4\times10^2 \rightarrow 8\times10^4$ ($1\text{x}10^5$ rare)	Biasing around orbit, but off for altitudes > 1200 km when near SAA. Ram angle at perigee 105°→74°. Emitter not on. APEX problems! No biasing 17 May-1 Jul.
31 Jul - 11 Aug 95	+50 V to +490 V	$2\times10^2 \rightarrow 3\times10^5$	Biasing around orbit, but off for altitudes > 1200 km when near SAA. Ram angle at perigee 78°→51°. Emitter not on. PASP+ controller problem 12 Aug! No more biasing.

Table IV. Summary of PASP Plus Negative Biasing Operations

Biasing Period	Voltage Range	Plasma Density (cm^{-3})	Environment and Operations Comments
22 Aug – 3 Sep 94	-75 V to -450 V	$\leq 6\times10^2 \rightarrow 6\times10^5$	No biasing in eclipse after 26 Aug. Higher negative voltages (−220V to −450V) only in sunlight. Unfavorable ram angles at perigee (111°→135°). TPM thresholds set at 0.
17 Oct – 22 Oct 94	-160 V to -400 V	$\leq 6\times10^2 \rightarrow 4\times10^5$	No eclipse period in orbits. Ram angle at perigee is ≤90° over 17-23 Oct (88°→73°). Arrays #2 and #1 are limited to −380V. TPM thresholds set at 0.
31 Oct – 4 Nov 94	-160 V to -370 V	$6\times10^2 \rightarrow 2\times10^5$	Eclipses return on 29 Oct. Ram angle at perigee 57°→53° in period. Arrays #2 and #1 limited to −300V (orbits include eclipse). TPM threshold at 0. APEX problem 4 Nov!
18 Jan – 11 Feb 95	-280 V to -460 V	$6\times10^3 \rightarrow 6\times10^5$ (some higher over 18–20 Jan)	Biasing only <1200 km. For APEX security, all Controller ops in sunlight until 4/5 Feb, then 10 min at end of eclipse. No significant eclipse meas. Ram angle at perigee 95°→64°. TPM threshold at 0 until 1 Feb, then set at 1.
3 Mar – 26 Mar 95 30 Mar – 1 Apr 95	-240 V to -430 V -240 V to -300 V	$6\times10^3 \rightarrow 8\times10^4$	Bias 12 min before to 42 min after perigee; this includes all of eclipse. Ram angle is ≤90° only past middle of eclipse. Ram angle at perigee 98°→176°. TPM threshold set at 1.
13 Apr – 18 Apr 95	-240 V to -370 V	$6\times10^3 \rightarrow 3\times10^5$	Bias 20 min before to 40 min after perigee; this includes all of eclipse. Ram angle is ≤90° only past middle of eclipse. Ram angle at perigee 143°→127°. TPM threshold set at 1.
1 Jul – 18 Jul 95	-300 V to -460 V	$2\times10^2 \rightarrow 4\times10^5$	Biasing around orbit, but off for altitude >1200 km when near SAA. Ram angle is ≤90° only past middle of eclipse. Ram angle at perigee 135°→109°. TPM threshold set at 1.
19 Jul – 30 Jul 95	-450 V to -500 V	$2\times10^2 \rightarrow 3\times10^5$	Biasing around orbit, but off for altitude >1200 km when near SAA. Ram angle is ≤90° only past middle of eclipse. Ram angle at perigee is 109°→80°. TPM threshold set at 1.

To explore plasma-environment effects on different array configurations, we tested arrays with small numbers of cells and achieved the high voltage levels needed through biases provided by the PASP Plus controller. We investigated leakage current enhanced by the "snapover" phenomenon for bias-simulated positive voltage operation and the rates of array arcing under bias-simulated negative voltage operation. From the variations in voltage level and in the space-environment conditions through which APEX flew, we were able to correlate (albeit imperfectly) the resultant interactions with the conditions imposed by nature and the experimental instrumentation.

Analysis of Positive Biasing Data

For arrays that are susceptible to the "snapover" phenomenon (the planar arrays), the "parasitic" or "leakage" current (I_{leak}) increases, as bias voltage and plasma density increase, by factors of 100 or more (even by as much as 1000 for planar arrays where snapover is initially suppressed by interconnect or side-edge shielding), as the entire array surface becomes engaged in current collection. The collecting area changes from the small areas of the cells' interconnects and side-edges to an area ultimately *larger* than the array's surface area, larger because current collection takes place in a plasma sheath that extends upward and outward from the biased array's surface.

We define a module's effective collecting area A_{coll} as the measured leakage current (Amp) divided by the thermal-plasma electron current density (Amp/m^2). $A_{coll} = I_{leak} / e\, n_e\, (\bar{v}/4)$; where e is the electron charge, n_e is the plasma density (measured by the experiment's Langmuir probe), and $n_e\, \bar{v}/4$ is the number of thermal electrons that would cross a unit area in unit time.[7] The average electron velocity $\bar{v}$ in a Maxwellian distribution is $(8kT_e / \pi m_e)^{1/2}$, where m_e is the electron mass and T_e is the electron temperature (also measured by the Langmuir probe).

The PASP Plus concentrator arrays (Modules #14 and #15) flown on APEX exhibited negligible leakage current over the whole range of plasma densities even for bias voltages up to +500 Volts.

To explore the effects of snapover, let us compare (for the purposes of this paper) the leakage current results for several different PASP Plus planar-array test modules. The data base used here includes all positive biasing data from 7 Aug 94 to 11 Aug 95 in sunlight and in the ram hemisphere (θ_{ram} = 0°→90°). In all cases, the experiment's electron emitter was off.

Figure 1 shows I_{leak} vs. applied positive bias (V_{bias}) for five binned levels of plasma density for four planar-array modules: #1, the old standard Si; #3, the Space-Station Si with wrap-through interconnects; #6, the somewhat older GaAs on Ge; and #8, the small GaAs on Ge array with wrap-through interconnects. The first three modules are of comparable total cell size (160, 256, and 192 cm^2), while the fourth module (#8) is quite small (64 cm^2).

Because of its highly exposed interconnects and side edges, Module #1 is collecting significant leakage current (1.5 to 45 μA, depending on n_e) at 50 V even without snapover. As V_{bias} is increased, secondary emission of electrons off the cells' coverglass surfaces causes them to be at positive potentials (snapover starts to set in). I_{leak} rises slowly at first (note the somewhat shallower slopes of the I_{leak} vs. V_{bias} curves in the 50–100 V range). The slopes then steepen and maximize in the 100–200 V range as the snapover-induced large changes in collecting area dominate. Beyond about 200–300 V (depending on n_e), the I_{leak} vs. V_{bias} curves flatten out (the collecting area maximizes) and I_{leak} no longer depends on V_{bias} but only the on the thermal electron flux, proportional to n_e and $T_e^{1/2}$ (T_e is much less important because of its limited range, 1000–6000 K in sunlit conditions).

Because of its "plasma shielding" wrap-through connectors and smaller cell-edge area (lessened cell-edge *perimeter* with just four large-area cells), Module #3 at 50 V collects very little leakage current, between 0.3 and 0.5 μA, with 0.2 μA being the electrometer's lower limit of measurement. As bias voltage is increased in the 50 to 100 V range, the I_{leak} vs. V_{bias} curves' slopes are steeper (on this log-log plot) than for Module #1 only because the Module #3 curves start off at such low I_{leak} values (Module #3's actual μA increases in I_{leak} are less than for Module #1). Then, as happened with Module #1, the slopes steepen and maximize in the 100–200 V range as the large changes in collecting area dominate. Beyond about 300–400 V, for the higher plasma densities ($\geq 10^{10}$ m^{-3}), the I_{leak} vs. V_{bias} curves start to flatten out as the collecting area maximizes and I_{leak} starts to depend mainly on n_e.

Module #6 has standard interconnects, but thinner and less exposed than Module #1. Its exposed cell-edge area (number of cells $\times$ cell perimeter $\times$ photovoltaic material thickness) is about a factor of three less than for Module #1. For the higher plasma densities (3×10^{10} and 10^{11} m^{-3}), Module #6 at 50 V, before snapover intervenes, collects modest leakage current (1.5 to 5 μA), about a factor of 10 less than Module #1, consistent with its smaller interconnect and cell-edge exposure. For the lower n_e values, 10^8 to 10^9 m^{-3}, Module #6 around 50 V collects surprisingly little I_{leak}, only 0.3 to 0.5 μA. [We have no explanation for these very low values, which approximate those of Module #3]. In the 50–100 V range, the slopes of the I_{leak} vs. V_{bias} curves increase gradually, then steepen and maximize in the 100–200 V range, as the large changes in collection area dominate, similar to Modules #1 and #3. The curves then flatten out in the 250–400 V range for the lower n_e curves and in the 350–500 V range for the higher n_e curves. After flattening out, the sets of I_{leak} vs. V_{bias} curves for Modules #1, #3 and #6 all asymptotically reach I_{leak} values similar to each other for the same n_e, but varying with n_e, roughly 18–22 μA for $n_e = 10^9$ m^{-3}, 75–85 μA for $n_e = 10^{10}$ m^{-3}, and 700–800 μA for $n_e = 10^{11}$ m^{-3}.

Module #8, GaAs on Ge with wrap-through connectors, is very small with only four 4$\times$4 cm cells. I_{leak} at 50 V is low, except for the $n_e = 10^{11}$ m^{-3} curve, which is probably in error due to the paucity of 50 V measurements with $n_e \approx 10^{11}$ m^{-3}. The slopes of Module #8's curves gradually increase in the 50–100 V range, steepen and maximize in the 100–200 V range, but then only start to turn over in the 300–500 range. Because of the limited cell area of this small module, the snapover-controlled I_{leak} never reaches the levels attained by Modules #1, #3 and #6, which draw current from a much more extensive plasma sheath.

The analysis presented here shows that once snapover is fully developed (as happened for Modules #1, #3 and #6), further increasing of the bias voltage would merely increases the negative floating potential of the spacecraft, so that the "array to plasma" voltage, which is actually responsible for the interactions, does not change appreciably. I_{leak} then depends almost exclusively on plasma density (more exactly on thermal electron flux, which includes a $T_e^{1/2}$ term, but with the small variation in T_e this term has little effect).

Let us examine the high-voltage end of the I_{leak} vs. V_{bias} curve sets for Modules #1, #3 and #6 shown in Figure 1. The I_{leak} curves flatten out as they reach values of 700–800 μA for $n_e = 10^{11}$m^{-3}. For the $n_e = 10^9$m^{-3} curves, I_{leak} reaches (or would reach when it fully flattens out) values of 18–22 μA. I_{leak} has about a 1½ order-of-magnitude variation with n_e, while n_e itself has a two order-of-magnitude variation, $10^9 \rightarrow 10^{11}$ m^{-3}. Thus, at the high-voltage end of the I_{leak} vs. V_{bias} curves where snapover is fully developed (Modules #1, #3 and #6 in Figure 1, but not #8), I_{leak} appears to be roughly proportional to $n_e^{0.75}$.

Since A_{coll} is *defined* with n_e to the first power in its denominator, while I_{leak} at the "snapover maximized" high-voltage end of the curve sets increases roughly as $n_e^{0.75}$, the collecting area (as we define it) at the high-voltage end should decrease with increasing plasma density (A_{coll} should be roughly proportional to $n_e^{-0.25}$).

Figure 2 shows A_{coll} vs. array-to-plasma voltage V_{A-P} for five binned levels (10^9 to 10^{10} m^{-3}) for Modules #1, #3, #6 and #8 (same modules as Figure 1). V_{A-P} is obtained by subtracting the magnitude of the spacecraft's negative "frame" potential V_{frame} (devived from ESA ion-channel data) from the applied positive bias (V_{bias}). The location of the energy *peak* (in eV) in the ESA's ion energy spectrum corresponds to V_{frame} in Volts. [Thermal ions arrive at the ESA's ion-channel aperture with an energy corresponding to V_{frame}.] For arrays where this effect is significant, V_{frame} is developed from available measurements (somewhat sparse) as a function of V_{bias} and n_e. The derived V_{frame} is subtracted from V_{bias} to obtain V_{A-P}. Even for the highest V_{bias} and n_e levels, V_{frame} is $<$100 V for Module #1, #3 and #6. For Module #8, V_{frame} is so small it cannot be derived, so $V_{A-P} = V_{bias}$.

Let us examine the high-voltage end of the A_{coll} vs. V_{A-P} curve sets for Modules #1, #3 and #6 in Figure 4. A_{coll} reaches (or would reach when it flattens out) values of 1.5-1.7 m^2, for $n_e = 10^9$m^{-3}, the *lowest* n_e curve. At $n_e = 10^{11}$m^{-3}, A_{coll} decreases to values of 0.50–0.58 m^2 for Modules #1, #3 and #6. There is about a one-half order-of-magnitude *decrease* in A_{coll} for the two order-of-magnitude increase in n_e. This result illustrates A_{coll}'s roughly $n_e^{-0.25}$ dependence on plasma density when snapover has become fully developed, and increases in positive bias voltage tend just to increase the negative frame potential. As for the small Module #8, it never reached fully-developed snapover at the highest bias levels of PASP Plus (V_{frame} was to low to measure), so no conclusions on n_e dependency for A_{coll} are possible.

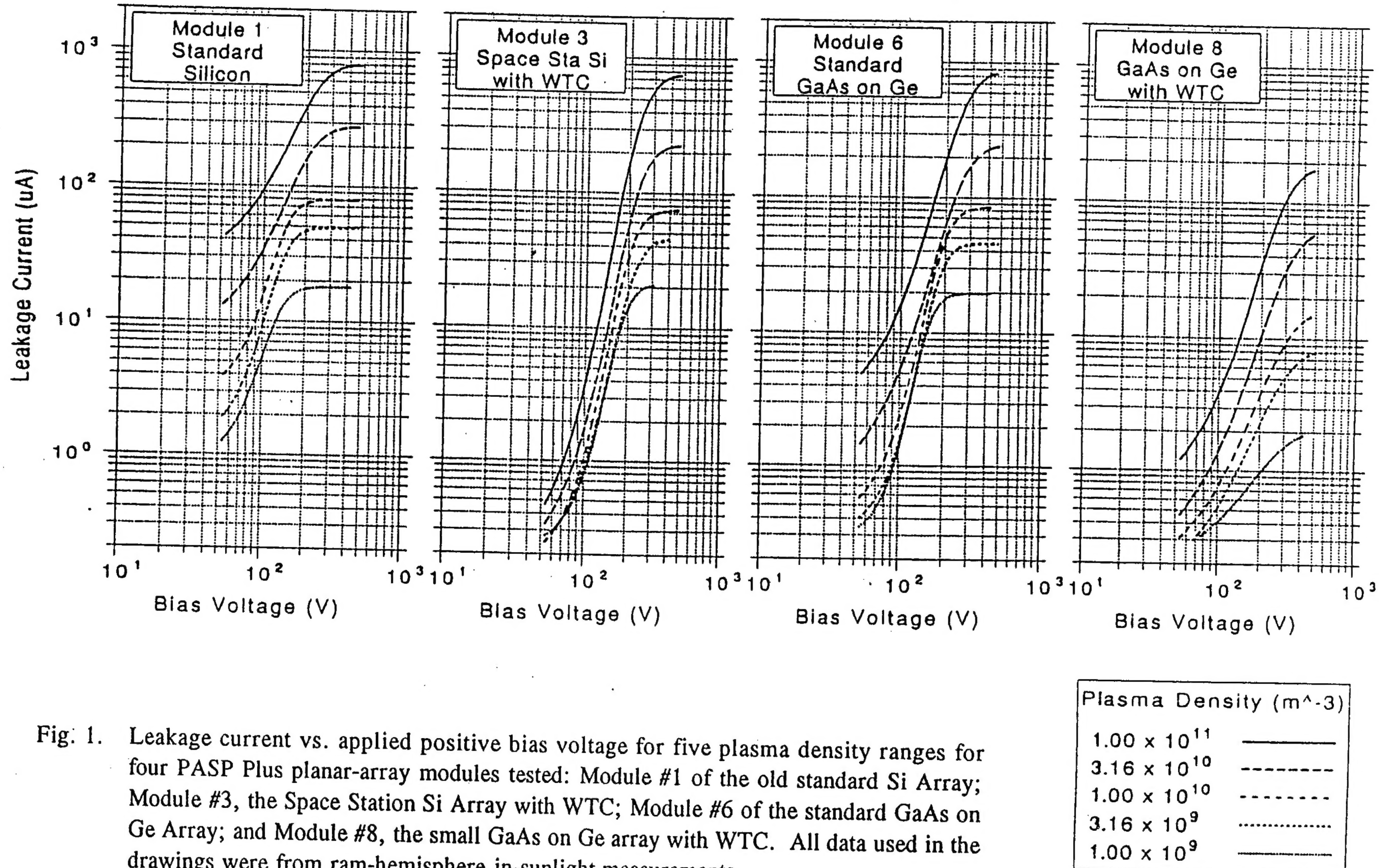

Fig. 1. Leakage current vs. applied positive bias voltage for five plasma density ranges for four PASP Plus planar-array modules tested: Module #1 of the old standard Si Array; Module #3, the Space Station Si Array with WTC; Module #6 of the standard GaAs on Ge Array; and Module #8, the small GaAs on Ge array with WTC. All data used in the drawings were from ram-hemisphere in-sunlight measurements.

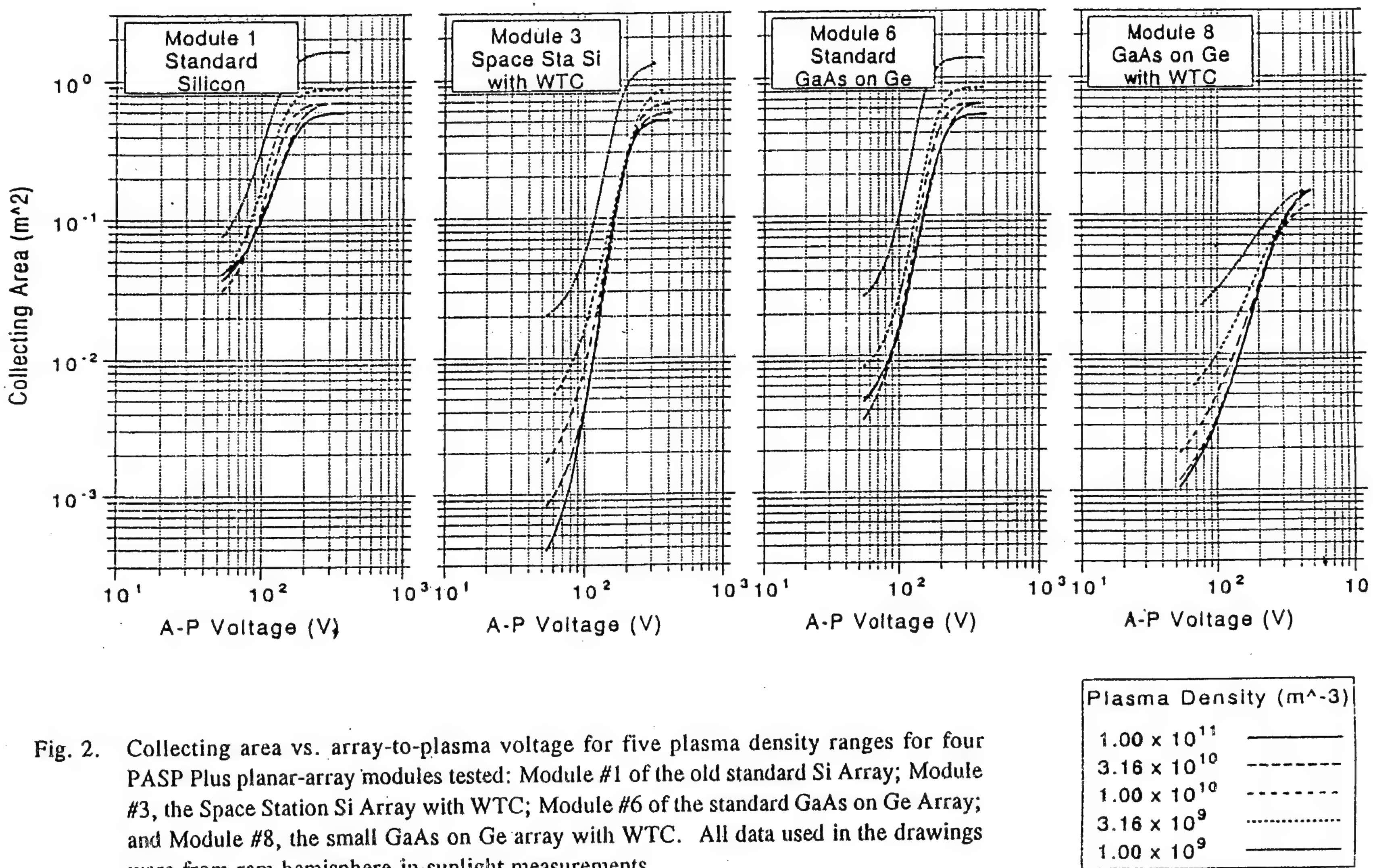

Fig. 2. Collecting area vs. array-to-plasma voltage for five plasma density ranges for four PASP Plus planar-array modules tested: Module #1 of the old standard Si Array; Module #3, the Space Station Si Array with WTC; Module #6 of the standard GaAs on Ge Array; and Module #8, the small GaAs on Ge array with WTC. All data used in the drawings were from ram-hemisphere in-sunlight measurements.

Analysis of Negative Biasing Data

The arc rates for PASP Plus's ten negatively biased test arrays were measured by the experiment's Transient Pulse Monitor (TPM) and the rates correlated with applied bias voltage and measured vehicle-orientation and environmental parameters. At this time there has been no analysis of the the other measured parameters of arcs (amplitude, derivative, or integral) with respect to bias voltage or flight-related conditions.

The concentrator arrays, due to the shielding of their cells from the space plasma, manifested no significant arcing during the course of our measurements, arcing at only the highest negative voltage levels, once at most in a biasing period, in less than 2% of the biasing trials. The very low number of trials where arcing took place made it impossible to study any dependencies.

The measured arc rate for the planar arrays showed a strong dependency on the mechanical configuration (i.e., metal interconnect and cell side-edge exposure to the space plasma). Analysis of PASP Plus measurements showed that planar arrays having their interconnects shielded from the space plasma have lower arcing rates. The arrays with wrap-through connectors have less arcs than would be expected based on other factors.

Modules #1 and #2 of the standard silicon array showed substantial arcing (even up to one arc per second) for voltages > 160 V, plasma densities $> 10^9\ m^{-3}$ in ram, both in sun and eclipse. This is to be expected since Array 0,1,2 is of old construction (exposed rough-surface interconnects). According to theory, if the interconnects have many field-emission sites (microscopically jagged regions with high electric-field enhancement factors), charging processes caused by enhanced-field electron emission can be initiated, leading to collisional ionization of neutral gas desorbed from the cell's coverglass, eventually resulting in an arc discharge.[8]

While Modules #1 and #2 showed much higher arc rates than the other arrays, the arc rate of all arrays showed a strong dependence on bias voltage. Arcing onset (threshold) voltages were found to be generally in the -100 V to -300 V range. See Table V for the experimentally measured and computer-simulated arcing onset voltages.

It was found that ion flux ($F_{ion} = n_{ion}\ v_{ion} \cos\theta_{ram}$) was also an important factor in determining arc rate. Access of the plasma's positive ions to the interactions volume between an array's solar cells is necessary for initiation of the sequence of interactions leading to arcing to occur. Figure 3 shows the measured arc rate dependence of Module #2 on bias voltage for a particular ion flux level ($10^{13}\ m^{-2}s^{-1}$). Figure 4 shows the arc rate dependence of Module #2 on ion flux for a particular bias voltage level (-300 V). Data points are shown by the filled and open circles in the figures. The curves drawn represent the best-fit exponential curves for the data set in each figure.

Table V. Arcing Onset Voltages: Experimental Measurements and Computer Simulations

Module/ Array Type	In-Space Measured Onset Voltage	Computer-Simulated Onset Voltage
1,2 Standard Silicon	−160 V	−160 V
3 Space Sta Si with wtc	−160 V	Not Derived
5 Thin Si (APSA)	−100 V to −125 V	−100 V
4,6 Standard GaAs on Ge	−125 V	−120 V
8 GaAs on Ge with wtc	−260 V to −300 V	Not Derived
11 GaAs on Ge	−180 V	−180 V

In general, arcing requires that the array *not* be in wake, in most cases this means $\theta_{ram} = \pm 90°$. However, for modules prone to arc (#1 and #2) it was observed that, at high negative biases especially in eclipse (cold is another arc enhancing factor), arcing occurred for the module near the edge of the deployed panel (Module #2) for ram angles up to nearly 120° while Module #1 in the center of the panel would not arc until θ_{ram} was $\leq 100°$ (with few arcs beyond 90°).

From negative-biasing data analysis, arcing was found to be more prevalent under cold array conditions, especially at the ends of eclipse periods. Based on theory, *cold* array temperatures would be expected to promote arcing: greater concentrations of neutral gas available for desorption and the gas staying in the interaction area (having less energy) under cold conditions. For thin arrays such as the APSA array (Module #5), temperature is an especially important arcing factor. While it was not biased beyond -300 V, Module #5's arcing was confined almost exclusively to eclipse periods where its temperature could reach −70C due to its very low mass and thermal isolation.

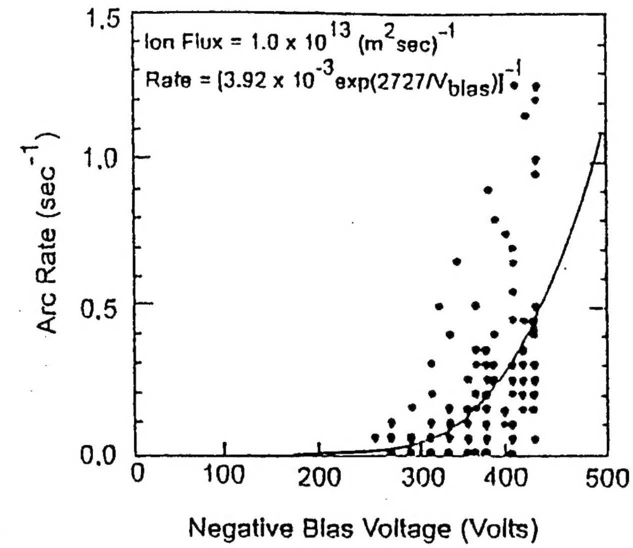

Fig. 3. Variation of Arc Rate with Applied Negative Voltage for Old Standard Si Module #2, Showing Data Points (filled circles) and Best-Fit Exponential Curve.

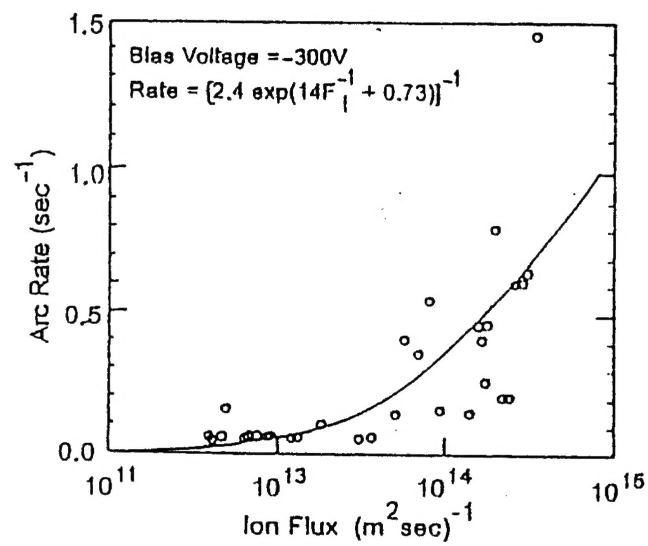

Fig. 4. Variation of Arc Rate with Ion Flux for Old Standard Si Module #2, Showing Data Points (open circles) and Best-Fit Exponential Curve.

These arc rates measured by PASP Plus have been compared with computer-generated simulations using a semi-analytic arc-rate code developed by M.I.T. for the experiment's conventional planar arrays.[8] The simulations were carried out using the measured "arc-rate determining" parameters (bias voltage, ion flux, array temperature, etc.) measured aboard APEX during negative biasing operations. Measured and simulated arc-rate findings were compared, with favorable results. The findings were subsequently used to develop cause-and-effect relationships and presented in a comprehensive report.[9]

Analysis of Radiation-Induced Degradation

PASP Plus obtained over 600,000 I–V curves for analysis, taking an I–V curve every 30 seconds except for eclipse periods and down times caused by APEX problems. In deriving the plots of P_{max} (or I_{sc} or V_{oc}) vs. days after launch for the different modules, we compensated for the 3.3% solar intensity variation (yearly earth-sun distance variation) and the variations caused by changes in array temperature. The latter was corrected using the P_{max}, I_{sc} and V_{oc} temperature coefficients from ground tests conducted at the Boeing test chamber at Kent WA.[10] The array temperatures gradually increased over the initial months of flight and then stabilized. This increase was likely caused by the lowered reflectivity of the Z-93 thermal-control paint on the payload shelf and deployed panel.

There is also a variation in I_{sc} (and hence in P_{max}) caused by variations in the "illumination" input from the earth's albedo. This illumination increase depends upon the angle between the satellite vertical and the earth-sun line. It also depends on the satellite altitude and earth surface viewed. Earth's albedo can add as much as 6% illumination to planar arrays. Because of their narrow viewing angle, concentrator arrays are immune to this effect. Albedo effects can lead to distortions in the day-to-day points on a P_{max} vs. days-from-launch plot, especially if the day's I–V curves are few (sometimes, only one). Nevertheless, the one-year trends display clear differences between the various PASP Plus arrays, as shown in Figures 5 through 9.

Modules #0 (Si), #4 (GaAs on Ge) and #10 (InP), shown in Figure 5, have similar cell-fabrication features (6-mil coverglasses and thick backs) but different cell materials. P_{max}, normalized to day zero (launch), shows a one-year degradation of 17% for the Si module and 13% for the GaAs on Ge module, but only 7.5% for the InP module, clearly showing InP's radiation hardness advantage.

Modules #3 (Space Station) and #5 (APSA) are examples of flexible Si-cell arrays. Each array is mounted on the deployed panel over a cut-out opening in the panel, causing them to have both their top and bottom surfaces open to the environment, as they would be in

operation as a prime power array on a large spacecraft. The one-year degradations for these modules, shown in Figure 6, were 21% for APSA and 24% for Space Station. For comparison, Figure 5 also shows the standard Si array, Module #0. The thin-cell (2.5 mil) APSA array degraded somewhat less than the thicker-cell (8 mil) Space Station array, even though APSA had less coverglass thickness (2.5 mil vs. 5 mil). It should be noted that the APSA and Space Station arrays were designed for lower orbits having much lower radiation.

The P_{max} degradation curve for Module #9, amorphous Si, is shown in Figure 7. For compactness, the vertical (P_{max}) scale of Figure 7 is compressed 2:1 compared to Figures 5, 6, 8 and 9. Module #9 showed the greatest P_{max} degradation: 42% in one year. While I_{sc} and V_{oc} each degraded about 12%, the majority of the P_{max} degradation came from a 25% drop in the fill factor ($ff = P_{max}/I_{sc} V_{oc}$). In contrast, the one-year degradation in fill factor for all the other test arrays was 1–2% or less. The P_{max} of amorphous Si module diminished 20% in 25 days and 32% in 75 days. The early part and most of the overall degradation is attributable to the solar-UV induced Stabler-Wronski effect. However, with a triple-junction amorphous Si cell, there may be some current mismatch effects as well. With 20-mil coverglass, the radiation-induced degradation for Module #9 would not be expected to be so high.[11]

Figure 8 shows the P_{max} degradation for Modules #7 and #12, the two dual-junction planar arrays. The AlGaAs//GaAs array with monolithic cells and the GaAs//$CuInSe_2$ array with mechanically stacked cells showed excellent radiation resistance, 9-10% for the one-year exposure. Since the photovoltaically generated voltages of the two parts of a dual-junction cell are different, their outputs have to be coupled so they are current matched (by controlling the doping and thicknesses of both materials) for monolithically grown cells or voltage matched (by combining the separate parts of the cell in a non-unity (e.g., 3:1) voltage ratio for mechanically stacked cells. The PASP Plus results indicate that radiation did not cause any significant "mismatching" losses in these arrays.

Figure 9 shows the P_{max} degradation for Module #15, the dual-junction GaAs//GaSb Mini-Dome concentrator array. With its cells protected by their Fresnel lenses, the Mini-Dome concentrator showed the least degradation, 7% over one year. For Module #14, the Mini-Cassegrainian concentrator array, because of internal cell problems, proper I–V curves could not be obtained, so no radiation degradation assessment could be made.

Conclusions

The PASP Plus experiment, despite the launch delays and the APEX problems in orbit, has provided outstanding space-research data to the solar-array community for the examination of space-plasma effects on high-voltage operation and space-radiation effects on long-term array power output. Through its August 1994 to August 1995 operation in space, PASP Plus collected an order of magnitude more data about environmental interactions on solar arrays than all previous space-borne photovoltaic experiments combined. The large data base gathered has allowed the development of cause-and-effect relationships. The experiment has permitted comparison of in-space measurements with analytic and computer-generated simulation models, leading to the use of the validated interaction codes to predict the performance of future solar arrays in particular space environments.

References

1. Grier, N.T., "Plasma Interaction Experiment II (PIX II): Laboratory and Flight Results", *Spacecraft Environmental Interactions Technology - 1983*, NASA CP-2359, AFGL-TR-85-0018, 1985, pp. 333-348.

2. Ferguson, D.C., "The Voltage Threshold for Arcing Solar Cells in LEO — Flight and Ground Test Results", AIAA 86-0362, 24th Aerospace Sciences Meeting, Reno, NV, 6–8 Jan. 1986.

3. Guidice, D.A., "PASP Plus: An Experiment To Measure Space-Environment Effects on Photovoltaic Power Subsystems", *Fifth Annual Workshop on Space Operations, Applications and Research (SOAR '91)*, NASA Conf. Publ. 3127, Vol.II, Feb. 92, pp. 662-668.

4. Guidice, D.A., Severance, P.S., Curtis, H.B., and Piszczor, M.F., "Investigation of Space-Environment Effects on Photovoltaic Technologies by the PASP Plus Experiment", AIAA 95-0371, 33rd Aerospace Sciences Meeting, Reno, NV, 9-12 Jan 1995.

5. Adams, S.F., "Photovoltaic Array Space Power Plus Diagnostics Flight Experiment: Pre-Flight Description of Experimental Photovoltaic Modules", WL-TR-92-2080, Wright Laboratory, Oct. 1992.

6. Guidice, D.A., "High-Voltage Space-Plasma Interactions Measured on the PASP Plus Test Arrays", *Proc. of XIV Space Photovoltaic Research and Technology Conf. (SPRAT XIV)*, NASA Conf. Publ. 10180, Oct. 1995, pp. 286–295.

7. Smiddy, M. and Stuart, R.D., "An Analysis of the Behavior of a Multi-Grid Spherical Sensor in a Drifting Maxwellian Plasma", AFCRL-69-0013, A.F. Cambridge Research Labs, Jan. 1969, p. 53.

8. Cho, M., and Hastings, D.E., "Dielectric Charging Processes and Arcing Rates of High-Voltage Solar Arrays," *J. Spacecraft & Rockets*, Vol. 28, 1991, pp. 698–706.

9. Soldi, J.D., and Hastings, D.E., "Arc Rate Simulation and Flight Data Analysis for the PASP Plus Experiment", PL-TR-95-2126, Phillips Lab., Sept. 1995.

10. Curtis, H.B., Guidice, D.A., Severance, P.S., and Piszczor, M.F., "Results of Thermal Vacuum Tests for the PASP Plus Flight Modules", *Proc. of XII Space Photovoltaic Research and Technology Conference*, NASA Conf. Publ. 3210, May 1993, pp. 289-297.

11. Curtis, H.B., and Marvin, D.C., "One Year of Flight Data from the PASP Plus Experiment", *Proc. of XIV Space Photovoltaic Research and Technology Conf. (SPRAT XIV)*, NASA Conf. Publ. 10180, Oct. 1995, pp. 268–273.

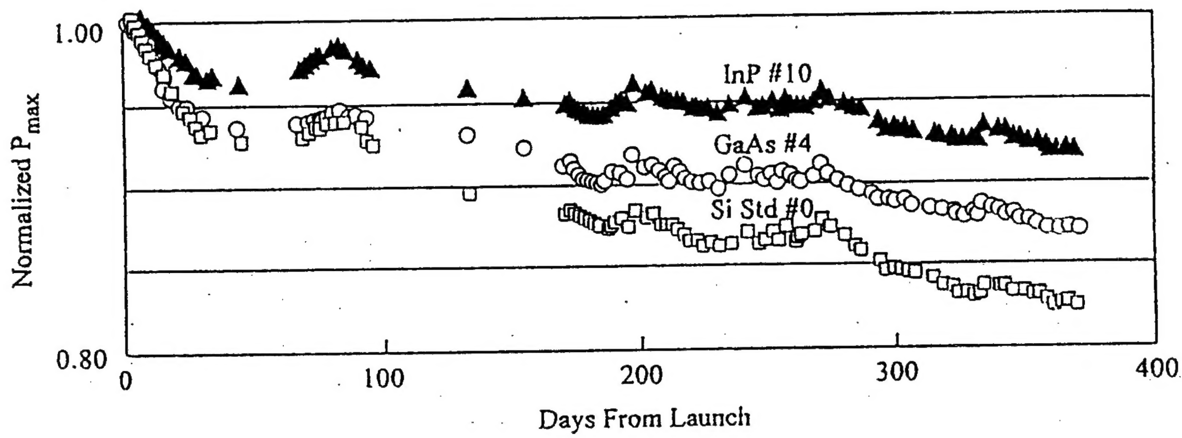

Fig. 5. Normalized P_{max} (Sun-Distance and Temperature Corrected) vs. Days from Launch for PASP Plus Test Modules #0 (Standard Si), #4 (GaAs on Ge), and #10 (InP). They have similar 6-mil coverglasses and thick backs.

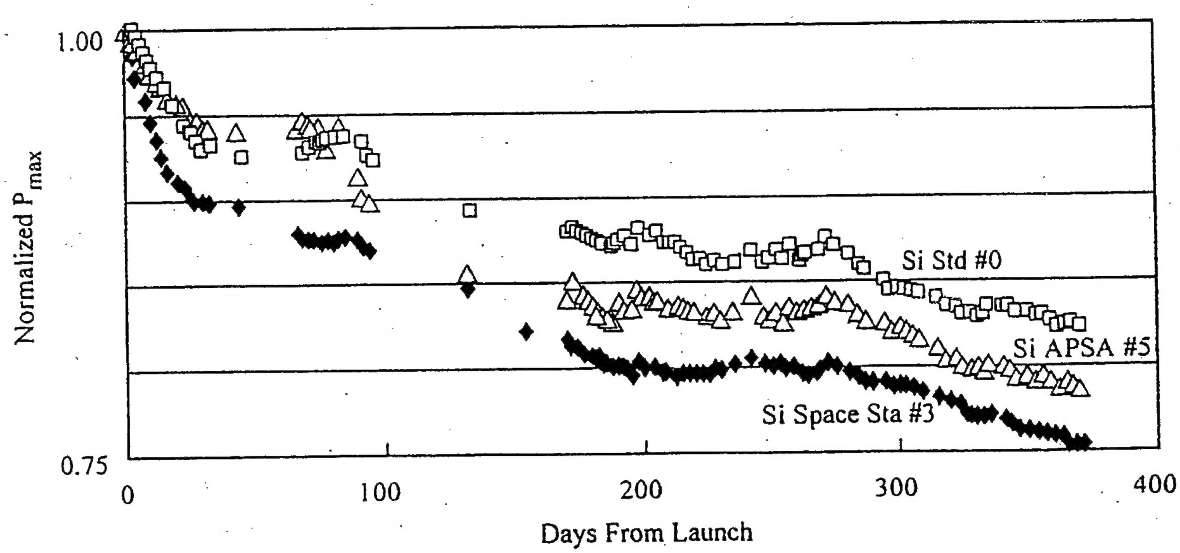

Fig. 6. Normalized P_{max} (Sun-Distance and Temperature Corrected) vs. Days from Launch for Modules #0 (Standard Si), #5 (the APSA Si array), and #3 (the Space Station Si Array).

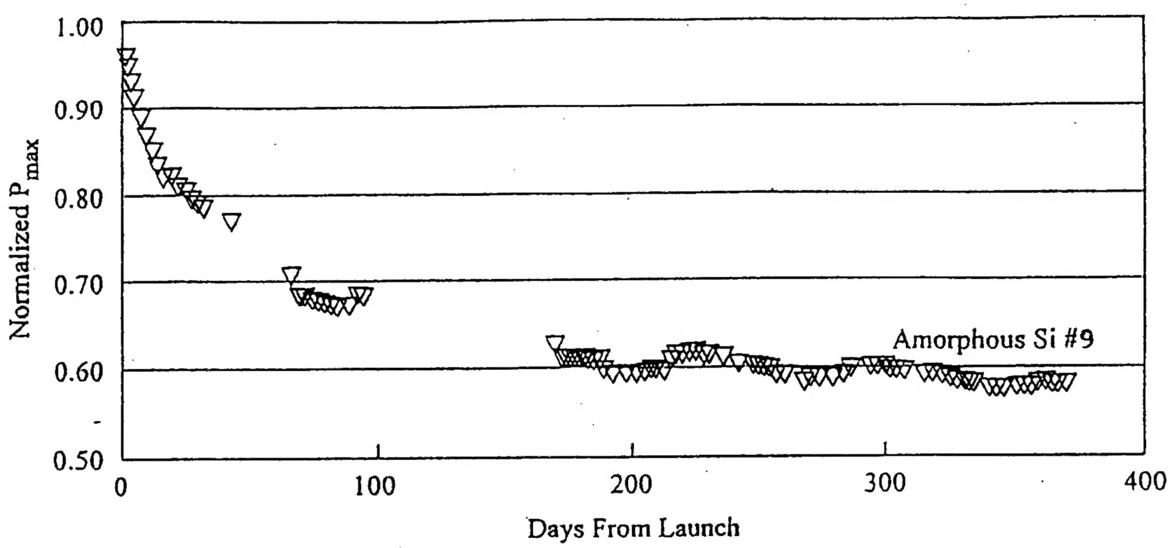

Fig. 7. Normalized P_{max} (Sun-Distance and Temperature Corrected) vs. Days from Launch for Module #9, Amorphous Si. The vertical (P_{max}) scale is compressed 2:1, compared to Figures 5, 6, 8 and 9.

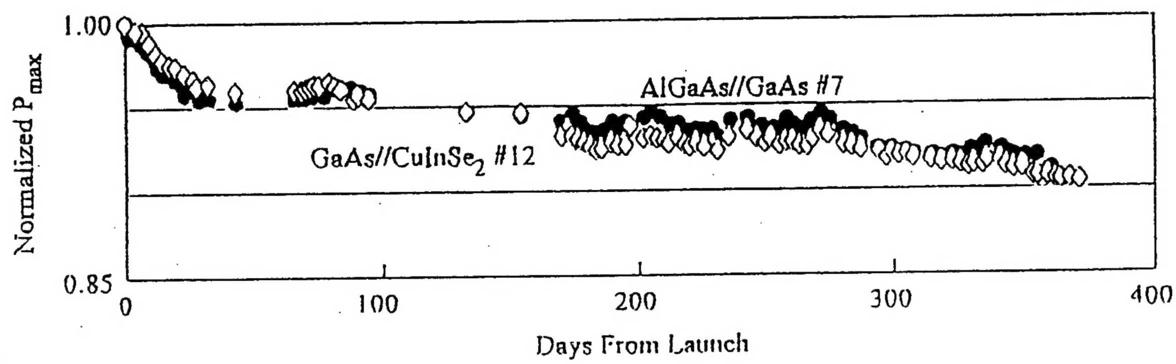

Fig. 8. Normalized P_{max} (Sun-Distance and Temperature Corrected) vs. Days from Launch for the Two Dual-Junction Planar Arrays. Module #7 is the AlGaAs//GaAs array with monolithic cells, and Module #12 is the GaAs//$CuInSe_2$ array with mechanically stacked cells.

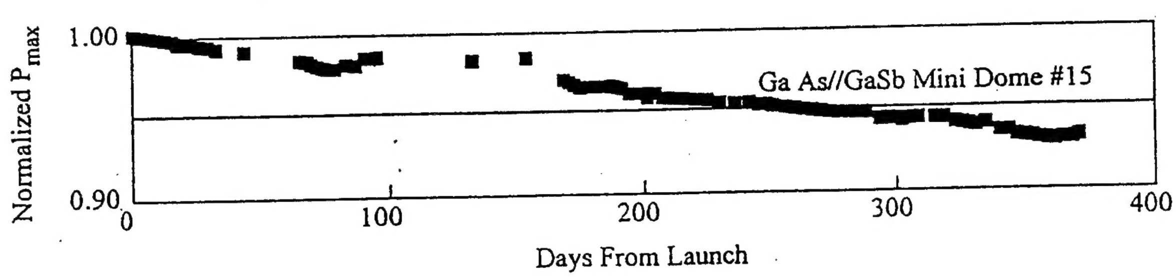

Fig. 9. Normalized P_{max} (Sun-Distance and Temperature Corrected) vs. Days from Launch for Module #15, the Dual-Junction GaAs//GaSb Mini-Dome Concentrator Array.